Eps15 membrane-binding and -bending activity acts redundantly with Fcho1 during clathrin-mediated endocytosis

Lei Wang, Adam Johnson, Michael Hanna, and Anjon Audhya*
Department of Biomolecular Chemistry, University of Wisconsin–Madison School of Medicine and Public Health, Madison, WI 53706

ABSTRACT **Clathrin coat assembly on membranes requires cytosolic adaptors and accessory proteins, which bridge triskeleons with the lipid bilayer and stabilize lattice architecture throughout the process of vesicle formation. In *Caenorhabditis elegans*, the prototypical AP-2 adaptor complex, which is activated by the accessory factor Fcho1 at the plasma membrane, is dispensable during embryogenesis, enabling us to define alternative mechanisms that facilitate clathrin-mediated endocytosis. Here we uncover a synthetic genetic interaction between *C. elegans* Fcho1 (FCHO-1) and Eps15 (EHS-1), suggesting that they function in a parallel and potentially redundant manner. Consistent with this idea, we find that the FCHO-1 EFC/F-BAR domain and the EHS-1 EH domains exhibit highly similar membrane-binding and -bending characteristics in vitro. Furthermore, we demonstrate a critical role for EHS-1 when FCHO-1 membrane-binding and -bending activity is specifically eliminated in vivo. Taken together, our data highlight Eps15 as an important membrane-remodeling factor, which acts in a partially redundant manner with Fcho proteins during the earliest stages of clathrin-mediated endocytosis.**

Monitoring Editor
Sandra Lemmon
University of Miami

Received: Mar 8, 2016
Revised: Jun 7, 2016
Accepted: Jun 29, 2016

INTRODUCTION

How particular subdomains of the plasma membrane are selected for clathrin-mediated endocytosis remains elusive. Nevertheless, numerous components have been implicated in the process, including the lipid phosphatidylinositol 4,5-bisphosphate (PI4,5P_2) and a large set of protein cofactors, several of which can bind and alter membrane topology while simultaneously recruiting clathrin and integral membrane substrates destined for internalization (Kaksonen *et al.*, 2005; Traub, 2009; Taylor *et al.*, 2011; Kirchhausen *et al.*, 2014). Perhaps the most central and best-characterized clathrin adaptor is AP-2, a heterotetrameric protein complex, which is regulated by members of the muniscin protein family (Fcho1, Fcho2, and SGIP1; Jackson *et al.*, 2010; Cocucci *et al.*, 2012; Umasankar *et al.*, 2014; Hollopeter *et al.*, 2014). Although the production of SGIP1 is largely restricted to neuronal cells, Fcho proteins are more ubiquitously expressed, and orthologues have been identified in most eukaryotic species (Katoh and Katoh, 2004; Trevaskis *et al.*, 2005; Reider *et al.*, 2009). In metazoans, Fcho proteins harbor three distinct regions: an amino-terminal EFC/F-BAR domain, which associates with PI4,5P_2-enriched lipid bilayers and induces membrane curvature; a central, unstructured linker motif, which allosterically promotes AP-2 activity; and a carboxyl-terminal mu homology domain (mu-HD), which functions as a protein interaction hub (Henne *et al.*, 2010; Umasankar *et al.*, 2014; Hollopeter *et al.*, 2014). In particular, the mu-HD binds avidly to the carboxyl terminus of Eps15, another endocytic accessory factor, which was identified originally as a substrate of epidermal growth factor receptor (EGFR) signaling and subsequently shown to be an important binding partner of the AP-2 α-adaptin subunit (Fazioli *et al.*, 1993;

This article was published online ahead of print in MBoC in Press (http://www.molbiolcell.org/cgi/doi/10.1091/mbc.E16-03-0151) on July 6, 2016.
The authors declare no conflicts of interest.
*Address correspondence to: Anjon Audhya (audhya@wisc.edu).
L.W., A.J., M.H., and A.A. conceived and designed the experiments. L.W., A.J., M.H., and A.A. performed experiments and analyzed data. L.W., A.J., M.H., and A.A. contributed reagents, materials, and analysis tools. L.W. and A.A. wrote the manuscript.
Abbreviations used: dsRNA, double-stranded RNA; EFC, extended FC; EGFR, epidermal growth factor receptor; EH, Eps15 homology; Fcho, Eps15 and intersectin, FEI; HA, hemagglutinin; MALS, multi-angle light scattering; mu-HD, mu homology domain; PI4,5P_2, phosphatidylinositol 4,5-bisphosphate; POPC, 1-palmitoyl-2-oleoyl-*sn*-glycero-3-phosphocholine; POPE, 1-palmitoyl-2-oleoyl-*sn*-glycero-3-phosphoethanolamine, POPS, 1-palmitoyl-2-oleoyl-*sn*-glycero-3-phospho-L-serine; PS, phosphatidylserine; Rhod-PE, 1,2-dipalmitoyl-*sn*-glycero-3-phosphoethanolamine-*N*-(lissamine rhodamine B sulfonyl); RNAi, RNA interference; SEC, size exclusion chromatography; SUPER, supported bilayers with excess membrane reservoir; TALEN, transcription activator-like effector nuclease.
© 2016 Wang *et al.* This article is distributed by The American Society for Cell Biology under license from the author(s). Two months after publication it is available to the public under an Attribution–Noncommercial–Share Alike 3.0 Unported Creative Commons License (http://creativecommons.org/licenses/by-nc-sa/3.0).
"ASCB®," "The American Society for Cell Biology®," and "Molecular Biology of the Cell®" are registered trademarks of The American Society for Cell Biology.

Benmerah *et al.*, 1996; Henne *et al.*, 2010; Umasankar *et al.*, 2014; Shimada *et al.*, 2016). Of note, the binding sites on Eps15 for Fcho proteins and AP-2 are nonoverlapping and noncompetitive. Eps15 also binds tightly to intersectin through a distinct coiled-coil region, and biochemical studies indicate that Fcho, Eps15, and intersectin can form a stable, independent complex (the FEI complex), which remains capable of associating with and activating AP-2 (Sengar *et al.*, 1999; Mayers *et al.*, 2013). Eps15 further binds to other factors that function in endocytosis through its amino-terminal Eps15 homology (EH) domains, including epsin, stonin, synaptojanin, and the ESCRT-0 complex (Haffner *et al.*, 1997; Chen *et al.*, 1998; Martina *et al.*, 2001; Mayers *et al.*, 2013). Despite the extensive catalogue of biochemical interactions identified, how this collection of factors works in unison to promote clathrin-mediated endocytosis remains unclear.

Genetic studies have played an important role in understanding how individual components of the endocytic machinery contribute to cargo internalization. Acute Eps15 inhibition in mammalian cell lines impairs EGFR and transferrin receptor endocytosis, but deletion of *Eps15* in murine fibroblasts fails to affect these pathways, suggesting that other proteins can compensate for its prolonged absence (Carbone *et al.*, 1997; Pozzi *et al.*, 2012). In other model organisms, including *Caenorhabditis elegans* and *Drosophila*, loss of Eps15 results in only cell type– and cargo-specific endocytic defects (Salcini *et al.*, 2001; Koh *et al.*, 2007). Acute or constitutive inhibition of Fcho similarly slows the kinetics of transferrin receptor internalization in cultured cells but fails to extinguish it (Cocucci *et al.*, 2012; Umasankar *et al.*, 2014). In zebrafish, loss of Fcho proteins perturbs embryonic development, largely due to inhibition of Bmp signaling, but does not result in the severe early embryonic phenotypes observed after depletion of the AP-2 α-subunit (Umasankar *et al.*, 2012). Even in the absence of AP-2 function, certain cargoes continue to be endocytosed, and, surprisingly, *C. elegans* that lack expression of the α-, σ-, or μ-subunit of AP-2 are viable and fertile (Conner and Schmid, 2003; Gu *et al.*, 2008, 2013; Mayers *et al.*, 2013). Collectively these data are consistent with the idea that a high level of plasticity exists in the endocytic machinery. In addition, these findings highlight a need for a wide range of endocytic adaptors and accessory factors with partially overlapping activities to ensure the timely removal of numerous distinct cargoes that display diverse and often degenerate sorting signals.

Consistent with work in cell lines, we and others have demonstrated that the single Fcho protein expressed in *C. elegans* (FCHO-1) is not essential for embryogenesis or animal viability (Mayers *et al.*, 2013; Hollopeter *et al.*, 2014). However, its absence phenocopies the loss of AP-2 subunits and results in endocytic defects that cause reduced body length, uncoordinated movement, and perturbations in cuticle morphogenesis and egg-laying (Hollopeter *et al.*, 2014). Phenotypes exhibited by *fcho-1* mutant animals are not substantially exacerbated by the additional loss of AP-2 subunits, suggesting that Fcho and AP-2 function largely in a common pathway. However, additional roles for Fcho that are independent of AP-2 have also been demonstrated (Stimpson *et al.*, 2009; Mayers *et al.*, 2013). Consistent with this idea, activation of AP-2 by the isolated central linker of FCHO-1 suppresses many of the morphological defects observed in *fcho-1* mutant animals but fails to fully suppress endocytic defects in individual cells (Hollopeter *et al.*, 2014). In contrast, the viability of *fcho-1* mutant embryos is dramatically reduced when Eps15 (EHS-1) and intersectin (ITSN-1) are also eliminated, suggesting that the individual components of the FEI complex act redundantly during endocytosis (Mayers *et al.*, 2013). Here we demonstrate that EHS-1 shares several of the properties exhibited by Fcho proteins, including the ability to bind and bend membranes. However, instead of acting to allosterically regulate AP-2, our findings suggest that EHS-1 functions in parallel with AP-2 to potentially scaffold a redundant adaptor system when Fcho and AP-2 functions are lacking.

RESULTS

Eps15 and intersectin play essential roles in the absence of Fcho1

Redundancy among endocytic cofactors has been convincingly illustrated in *C. elegans*, in which none of the known clathrin adaptors is individually essential for embryo viability (Sönnichsen *et al.*, 2005). In contrast, clathrin heavy chain is absolutely required early during embryonic development, and its depletion results in 100% embryo lethality (Figure 1A). To exploit the functional redundancy in *C. elegans* clathrin adaptors and accessory proteins, we conducted a focused genetic screen based on the idea that when specific mutations are combined, synthetic genetic interactions can reveal components that function in parallel, synergistic pathways, which are essential for growth. Constitutive loss of *FCHO-1* causes approximately ~8% (±3%) of embryos to arrest before hatching (Figure 1A), whereas the remaining animals progress to adulthood, exhibiting a variety of morphological defects that have been described earlier (Hollopeter *et al.*, 2014). Using RNA interference (RNAi), we depleted each of the conserved clathrin adaptors and accessory proteins in worms harboring a null mutation in *FCHO-1*. Our screen revealed two strong genetic interactions that led to a significant reduction in embryo viability. Specifically, we found that inhibition of EHS-1 (Eps15) or ITSN-1 (intersectin) in *fcho-1* mutant animals resulted in ~40% (±5%) and ~21% (±5%) embryonic lethality, respectively, whereas elimination of these factors in control animals failed to elicit a significant effect on embryo viability (Figure 1, A and B). To confirm these genetic interactions, we created *fcho-1/ehs-1* and *fcho-1/itsn-1* double-mutant animals. Consistent with our RNAi depletion-based studies, both double mutants exhibited significantly elevated embryonic lethality compared with individual single-mutant strains (Figure 1B). As controls, we also generated several other double-mutant animals, including animals lacking HIPR-1 or AMPH-1 in the *fcho-1* mutant background. In none of these cases did we observe a significant elevation in embryo lethality relative to the single-mutant animals, further suggesting that the genetic interactions we identified in our small-scale screen were specific (Figure 1B). Together these data are consistent with the idea that FCHO-1 shares an essential, overlapping function with EHS-1 and ITSN-1 during early embryo development.

Previous studies demonstrated that EHS-1 and ITSN-1 interact with one another via their central coiled-coil motifs and form a stable, evolutionarily conserved complex in vivo and in vitro (Sengar *et al.*, 1999; Mayers *et al.*, 2013). Null mutations in each do not significantly affect *C. elegans* embryo viability, and *ehs-1/itsn-1* double-mutant animals fail to exhibit a synthetic genetic interaction (Figure 1B). However, prior work showed that the protein stability of ITSN-1 is compromised in the absence of EHS-1, which further suggests that the pair functions as an integrated, codependent unit (Wang *et al.*, 2008). We therefore questioned why *fcho-1/ehs-1* and *fcho-1/itsn-1* double-mutant animals exhibit distinct phenotypes (~42 vs. ~25% lethality) during embryo development. Given the destabilizing effect of eliminating EHS-1 on ITSN-1 levels, we decided to measure the stability of EHS-1 in *itsn-1*-null mutants and determine whether the reciprocal is also true. Surprisingly, we found that EHS-1 protein levels were not affected in this mutant background (Figure 1C). Moreover, whereas we failed to observe the normal accumulation of ITSN-1 at the plasma membrane in *ehs-1* mutant

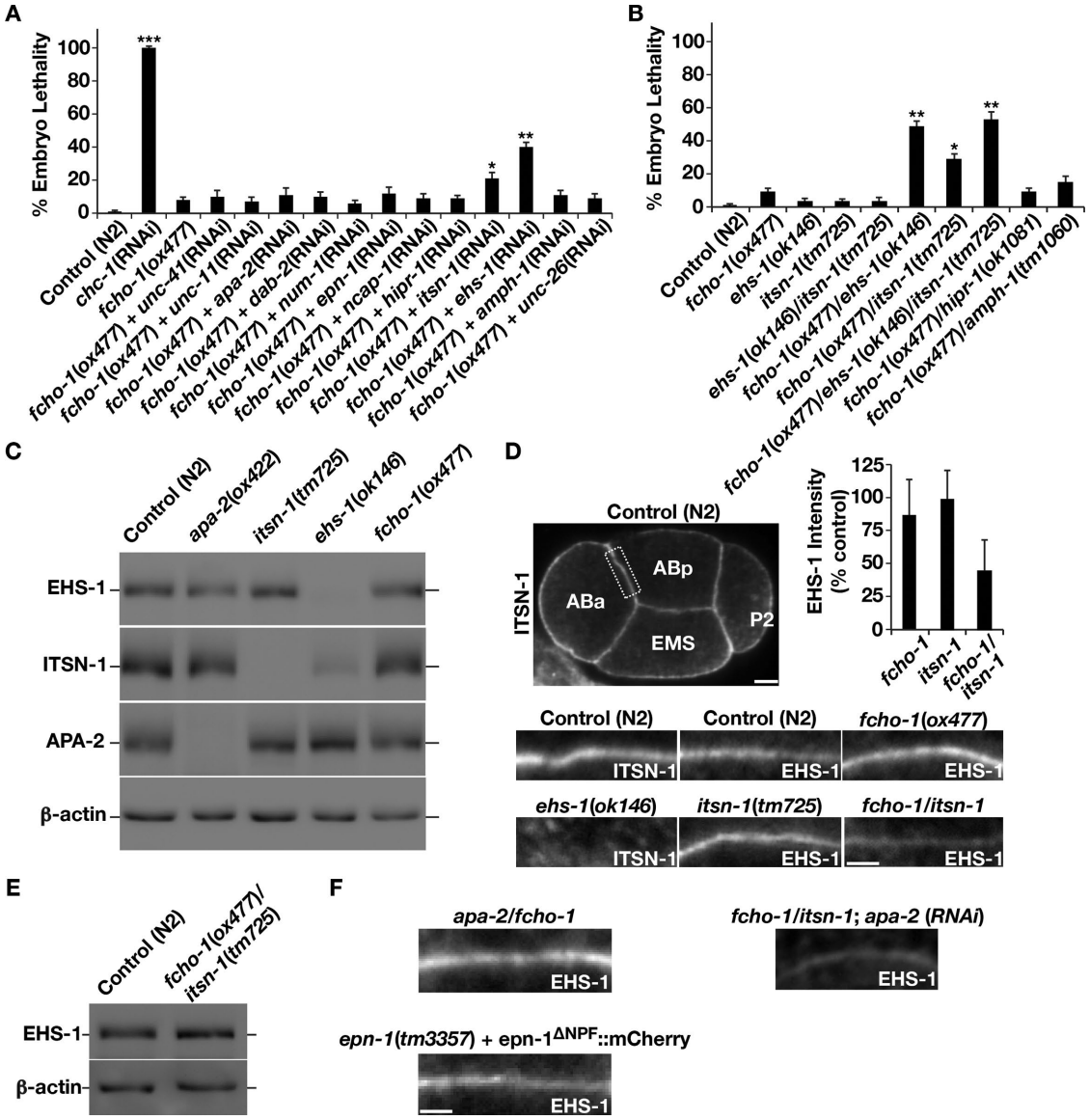

FIGURE 1: Small-scale synthetic genetic interaction screen reveals a potential overlapping function between FCHO-1 and EHS-1 in *C. elegans*. (A) Control and *fcho-1*(*ox477*) animals at the early L4 stage of development were soaked for 24 h with dsRNAs targeting known components of the endocytic machinery in *C. elegans*. After 48 h of recovery, hermaphrodites were moved to individual plates and allowed to lay eggs for 24 h. The percentage that failed to hatch in each case was calculated, and all experiments were repeated at least five times. Error bars represent mean ± SEM. ***$p < 0.001$ compared with control; **$p < 0.01$ compared with *fcho-1*(*ox477*) animals; *$p < 0.05$ compared with *fcho-1*(*ox477*) animals; each calculated using a paired *t* test. (B) Control and single- and double-mutant animals were segregated individually onto plates as synchronized adults and allowed to produce progeny for 24 h. The percentage of embryos that failed to hatch was determined in each case, and all experiments were repeated at least five times. Error bars represent mean ± SEM; five replicates each. **$p < 0.01$ compared with *fcho-1*(*ox477*) animals, and *$p < 0.05$ compared with *fcho-1*(*ox477*) animals, calculated using a paired *t* test. (C) Gravid adults ($n = 30$) of each genotype indicated were pooled and solubilized in SDS-containing sample buffer. Boiled extracts were resolved by SDS–PAGE and immunoblotted using the antibodies indicated. Data shown are representative of three independent experiments. (D) Dissected embryos of the genotypes indicated were fixed and stained using dye-labeled EHS-1 or ITSN-1 antibodies. The plasma membranes between the ABa and ABp cells (top, boxed area) are shown in each case. Scale bars, 5 µm (whole embryo), 2 µm (magnified areas). Top, right, relative intensity of EHS-1 staining in *fcho-1*, *itsn-1*, and *fcho-1*/*itsn-1* mutant four-cell-stage embryos, calculated as a percentage of control (N2) embryos. Data are representative of three independent experiments for each condition (at least four embryos analyzed in each experiment). (E) Gravid adults ($n = 30$) of each genotype indicated were pooled and solubilized in SDS-containing sample buffer. Extracts were resolved by SDS–PAGE and immunoblotted using the antibodies indicated. Data shown are representative of three independent experiments. (F) Dissected embryos of the genotypes indicated were fixed and stained using dye-labeled EHS-1 or ITSN-1 antibodies. The plasma membranes between the ABa and ABp cells are shown in each case. Scale bar, 2 µm. Data are representative of three independent experiments for each condition (at least four embryos analyzed in each experiment).

embryos, the localization of EHS-1 was unaffected by the loss of ITSN-1 (Figure 1D). Together our data suggest that the presence of ITSN-1 does not regulate EHS-1 stability or distribution in vivo. In addition, these findings offer a plausible explanation for the milder phenotype exhibited by *fcho-1/itsn-1* double-mutant animals compared with *fcho-1/ehs-1* double-mutant animals. Specifically, the continued presence of EHS-1 likely promotes improved survival of *fcho-1/itsn-1* double-mutant embryos. Consistent with this possibility, deletion of *EHS-1* in the *fcho-1/itsn-1* mutant background significantly increases the level of embryonic lethality (Figure 1B; Mayers *et al.*, 2013).

If the presence of EHS-1 enhances embryo survival in the absence of FCHO-1 and ITSN-1, we questioned why there exists any genetic interaction between the *fcho-1* and *itsn-1* null alleles. Previous work indicates that FCHO-1 associates directly with EHS-1 in a complex that also contains ITSN-1, raising the possibility that EHS-1 is regulated by its interaction partners (Henne *et al.*, 2010; Mayers *et al.*, 2013). To address this idea, we examined how the loss of FCHO-1 and the simultaneous loss of FCHO-1 and ITSN-1 affect EHS-1 protein levels and distribution in cells. Immunoblot analysis of whole-animal extracts indicated no change in EHS-1 protein stability in *fcho-1* mutant animals, and EHS-1 localization to the plasma membrane was normal in this genetic background (Figure 1, C and D). When both FCHO-1 and ITSN-1 were absent, EHS-1 stability was similarly unaffected (Figure 1E). However, we observed a reproducible decrease in the plasma membrane localization of EHS-1 in *fcho-1/itsn-1* double-mutant embryos, although it remained capable of targeting to the cell surface (Figure 1D). These data suggest that the reduced recruitment of EHS-1 to the plasma membrane in *fcho-1/itsn-1* double-mutant animals might underlie the genetic interaction observed. Furthermore, our findings highlight a redundant, overlapping function for FCHO-1 and ITSN-1 in regulating the cell surface distribution of EHS-1 in vivo.

We next sought to understand how EHS-1 remains capable of membrane accumulation even when two of its major binding partners are absent. Unlike FCHO-1, which harbors an EFC/F-BAR domain that is known to interact with PI4,5P_2 and other cell surface–enriched acidic phospholipids, EHS-1 has not been shown to harbor a motif that functions similarly. We first considered whether the α-subunit of the AP-2 adaptor complex (APA-2 in *C. elegans*) might participate in this process, since it was shown previously to associate directly with EHS-1 (Benmerah *et al.*, 1996). To test this idea, we examined the distribution of EHS-1 in animals lacking APA-2 but found no defect in EHS-1 membrane targeting. Similarly, *fcho-1/apa-2* double-mutant embryos exhibited a normal distribution of EHS-1 at the cell surface (Figure 1F), and EHS-1 stability was unaffected by the absence of APA-2 (Figure 1C). We also examined EHS-1 plasma membrane localization in *fcho-1/itsn-1* mutant embryos depleted of APA-2 and found that its accumulation was not further affected compared with *fcho-1* single-mutant embryos (Figure 1F). Finally, we tested potential roles for several other endocytic adaptors, including EPN-1 (epsin), which binds to EHS-1 via its EH domains (Chen *et al.*, 1998), in facilitating EHS-1 membrane association but failed to identify any potential regulators (Figure 1F). Together these data raise the possibility that EHS-1 can target to membranes independently of a protein cofactor.

The Eps15 tandem EH domain functions similarly to the Fcho1 EFC/F-BAR domain

Based on chemical shift experiments using nuclear magnetic resonance, previous work suggested that EHS-1 might be capable of binding directly to membranes (Naslavsky *et al.*, 2007). In particular, the second EH domain was found to associate with PI3,5P_2, a phosphoinositide lipid enriched in the late endosomal system (Dove *et al.*, 2009). In contrast, we showed previously that EHS-1, together with ITSN-1 and FCHO-1, associates specifically with the plasma membrane in *C. elegans* embryos (Mayers *et al.*, 2013). To revisit the question of whether EHS-1 binds directly to membranes, we conducted a series of coflotation experiments with synthetic liposomes composed of different lipid mixtures. Whereas we observed minimal binding to membranes harboring only neutral lipids, the addition of two negatively charged phospholipids, phosphatidylserine (PS) or PI4,5P_2, which are enriched in the plasma membrane, increased EHS-1 membrane association (Figure 2A). We also tested the ability of full-length FCHO-1 and ITSN-1 to interact with membranes and found that they both exhibited a preference for liposomes containing PS and PI4,5P_2 (Figure 2A). Together these data indicate that all three components of the FEI complex interact with negatively charged membranes.

Given the similar lipid-binding profiles exhibited by components of the FEI complex, we entertained the possibility that one of the redundant functions shared between FCHO-1, EHS-1, and ITSN-1 is membrane binding and bending, which may play an important role during the initial stages of clathrin-coated pit formation. Previous work showed that a mutant form of FCHO-1 that lacks its EFC/F-BAR domain fully rescues all phenotypes associated with the *fcho-1* null mutation in *C. elegans*, suggesting that other factors are capable of membrane sculpting or remodeling during the early phases of endocytic pit formation (Hollopeter *et al.*, 2014). To address this possibility, we first sought to specify the lipid-binding modules within EHS-1 and ITSN-1. Given their similar lipid-binding profiles, we speculated that they share a common motif, which mediates an association with membranes. Both proteins contain coiled-coil motifs, which associate with one another, and EH domains that are recognized partners for NPF-containing endocytic factors (de Beer *et al.*, 2000). Based on the previous work showing that the second Eps15 EH domain can interact with PI3,5P_2 in vitro (Naslavsky *et al.*, 2007), we focused our attention on the tandem EH domains present in both EHS-1 and ITSN-1. These regions were purified recombinantly and assayed for membrane association by coflotation using liposomes containing 15% PS and 3% PI4,5P_2. In comparison to the well-characterized FCHO-1 EFC/F-BAR domain, the pair of EH domains in ITSN-1 was retained on membranes to a lesser extent (Figure 2B). In contrast, the triplet of EH domains in EHS-1 cofloated with liposomes similarly to the FCHO-1 EFC/F-BAR domain (Figure 2B). To examine the evolutionary conservation of EH domain–mediated membrane association, we also purified the tandem EH domains from mouse Eps15 and found that this region exhibited a similar degree of membrane binding as EH domains from *C. elegans* EHS-1 (Figure 2B). In both cases, we observed a strong preference for membranes containing both PS and PI4,5P_2, even when compared with liposomes exhibiting an equivalent charge but only containing PS (Figure 2C). In contrast, the carboxyl-terminal EH domain from RME-1 failed to exhibit comparable binding (Figure 2C), suggesting that amino-terminal, tandem EH domains exhibit unique properties relative to carboxyl-terminal EH domains.

To narrow which of the three EHS-1 EH domains contribute to membrane binding, we purified them individually (EH1 and EH3) and as tandem pairs (EH1-EH2, EH2-EH3), with the exception of the second EH domain alone (EH2), which was insoluble. Whereas we failed to observe an interaction between EH1 and liposomes, the other fragments cofloated, with the tandem EH2-EH3 pair associating best with membranes, albeit not as well as the intact triplet of EH domains (Figure 2D). These data suggest that the three EH domains in EHS-1

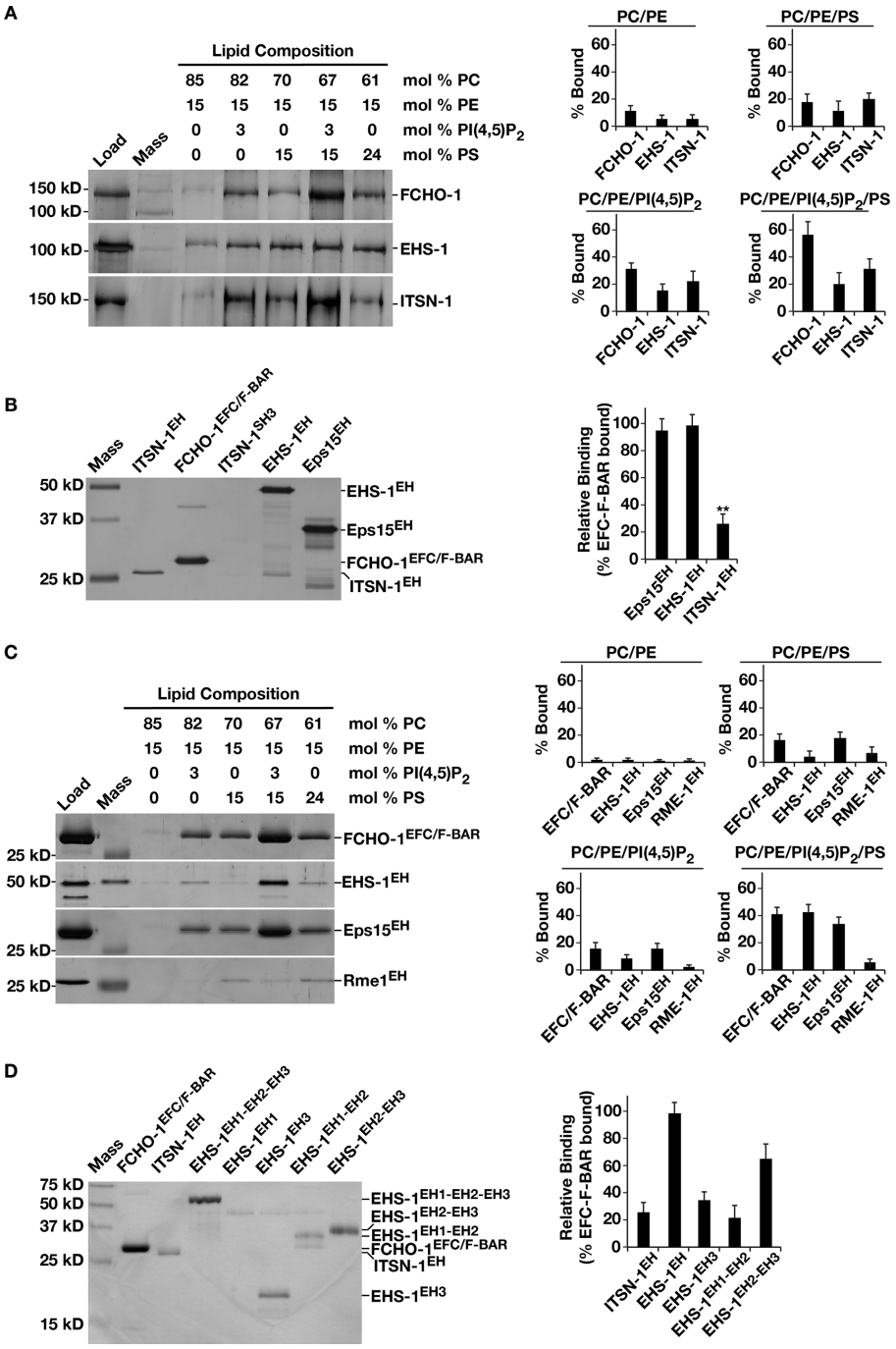

FIGURE 2: The Eps15 EH domain exhibits a preference for binding to negatively charged lipids. (A) A coflotation assay was used to analyze the binding of recombinant full-length FCHO-1 (100 nM), EHS-1 (200 nM), or ITSN-1 (200 nM) to liposomes (3 mM) of varying composition. Liposome-bound proteins were resolved by SDS–PAGE and silver stained. The amount recovered under each condition (percentage bound) was calculated as a percentage of the total protein used in each assay. Only a fraction of the total (10–40%) was loaded onto the gel for comparison (Load). Lane 2 in each case contains a molecular mass marker (Mass). Data shown are representative of more than three independent experiments. (B) A coflotation assay was used to analyze binding of the recombinant proteins indicated (600 nM each) to liposomes (3 mM) composed of 67% POPC, 15% PE, 3% PI4,5P_2, and 15% PS. Liposome-bound proteins were resolved by SDS–PAGE and silver stained. Relative binding of each domain was calculated as a percentage of the FCHO-1 EFC/F-BAR domain that was recovered. Data shown are representative of more than three independent experiments. (C) A coflotation assay was used to analyze binding of the recombinant proteins indicated (600 nM each) to liposomes (3 mM) of varying composition. Liposome-bound proteins were resolved by SDS–PAGE and silver stained. The amount recovered under each condition (percentage bound) was calculated as a percentage of the total protein used in each assay. Only a fraction of the total (10–40%) was loaded onto the gel for comparison (Load). Lane 2 in each case contains a molecular mass marker (Mass). Data shown are representative of more than three independent experiments. (D) A coflotation assay was used to analyze binding of the recombinant proteins indicated (86 nM each) to liposomes (3 mM) composed of 67% POPC, 15% PE, 3% PI4,5P_2, and 15% PS. Liposome-bound proteins were resolved by SDS–PAGE and silver stained. Relative binding of each domain was calculated as a percentage of the FCHO-1 EFC/F-BAR domain that was recovered. Data shown are representative of more than three independent experiments.

are not functionally equivalent with regard to membrane binding.

The Eps15 tandem EH domain binds to PI4,5P_2 in cells

To further examine the preference of the EHS-1 EH domains for PI4,5P_2 compared with PS, we expressed it as a green fluorescent protein (GFP) fusion in human RPE1 cells. Consistent with an ability to recognize NPF-containing endocytic adaptors, the *C. elegans* EH domains accumulated at clathrin-coated structures at or near the cell cortex in the majority of cases (Figure 3A). However, we also observed significant accumulation of the fusion protein throughout the cytoplasm, suggesting that its affinity for clathrin-coated pits was relatively modest. To eliminate NPF recognition, we mutated a key tryptophan residue in each EH domain to glycine (EH^{3WG}) (de Beer *et al.*, 2000). When this mutant form of the *C. elegans* tandem EH domain was expressed at low levels in cells, we found that it was redistributed around the entire plasma membrane in most cells, although we continued to observe its accumulation in the cytoplasm as well (Figure 3B). To test whether its cell surface localization was dependent on PI4,5P_2, we coexpressed a doxycycline-inducible form of the bacterial PI 5-phosphatase SigD (Terebiznik *et al.*, 2002). On addition of doxycycline to the medium, we found that the EHS-1 EH^{3WG} domain was released from the plasma membrane (Figure 3C). Similarly, the wild-type EHS-1 EH domain was also largely dependent on PI4,5P_2 for its localization to cell surface clathrin-coated structures, as was the distribution of the σ-subunit of the mammalian AP-2 complex (Figure 3, D and E). In contrast, expression of SigD did not affect the plasma membrane levels of PS (Figure 3, E and F), and a mutant form of SigD that lacks phosphatase activity (C462S)

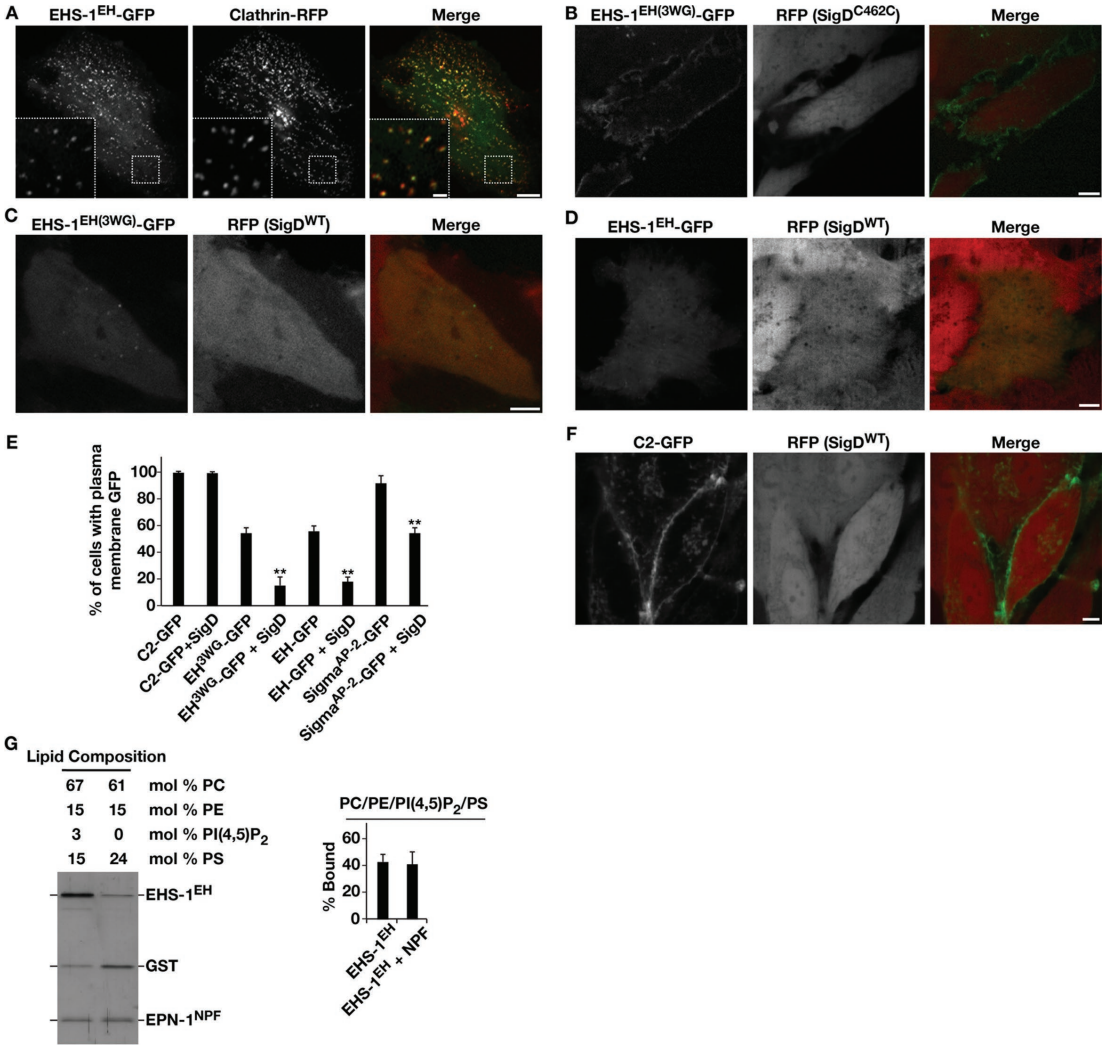

FIGURE 3: The *C. elegans* EHS-1 EH domain associates simultaneously with PI4,5P_2- and NPF-containing proteins in human cells. (A) RPE1 cells stably expressing low levels of the EHS-1 tandem EH domain as a GFP fusion were transiently transfected with a plasmid encoding clathrin light chain fused to monomeric RFP and imaged using swept-field confocal optics at the cell cortex. Scale bar, 5 µm. Bottom, left, higher-magnification views of the indicated regions (boxed); scale bar, 1 µm. Data shown are representative of >30 cells imaged in three independent experiments. (B) RPE1 cells stably expressing low levels of an EHS-1 tandem EH domain fused to GFP, which is unable to associate with NPF motif–containing proteins (3WG), were treated with doxycycline (10 ng/ml) to induce expression of a phosphatase-inactive form of SigD for 24 h and imaged live using swept-field confocal optics at a medial plane. RFP fluorescence serves as an indicator of SigD expression. Scale bar, 5 µm. Data shown are representative of >30 cells imaged in three independent experiments. (C) RPE1 cells stably expressing low levels of an EHS-1 tandem EH domain fused to GFP, which is unable to associate with NPF motif–containing proteins, were treated with doxycycline (10 ng/ml) to induce expression of an active form of SigD for 24 h and imaged live using swept-field confocal optics at a medial plane. RFP fluorescence serves as an indicator of SigD expression. Scale bar, 5 µm. Data shown are representative of >30 cells imaged in three independent experiments. (D) RPE1 cells stably expressing low levels of the EHS-1 tandem EH domain fused to GFP were treated with doxycycline (10 ng/ml) to induce expression of an active form of SigD for 24 h and imaged live using swept-field confocal optics at a cortical plane. RFP fluorescence serves as an indicator of SigD expression. Scale bar, 5 µm. Data shown are representative of >30 cells imaged in three independent experiments. (E) Quantification of the number of cells exhibiting plasma membrane GFP fluorescence in the presence or absence of active SigD. Error bars represent mean ± SEM. $^{**}p < 0.01$, calculated using a paired *t* test, comparing genetically identical cells with and without active SigD expression. At least 100 different cells per condition were analyzed. (F) RPE1 cells stably expressing low levels of the lactadherin C2 domain fused to GFP were treated with doxycycline (10 ng/ml) to induce expression of an active form of SigD for 24 h and imaged live using swept-field confocal optics at a medial plane. RFP fluorescence serves as an indicator of SigD expression. Scale bar, 5 µm. Data shown are representative of >30 cells imaged in three independent experiments. (G) A coflotation assay was used to analyze binding of the EHS-1 tandem EH domain to liposomes of varying composition. The EPN-1 NPF domain (300 nM) was purified initially as a GST fusion protein and cleaved using Precision protease before incubation with the EHS-1 tandem EH domain (300 nM) and liposomes (3 mM). Liposome-bound proteins were resolved by SDS–PAGE and silver stained. The amount recovered under each condition (percentage bound) was calculated as a percentage of the total protein used in each assay (as in Figure 2C). Data shown are representative of more than three independent experiments.

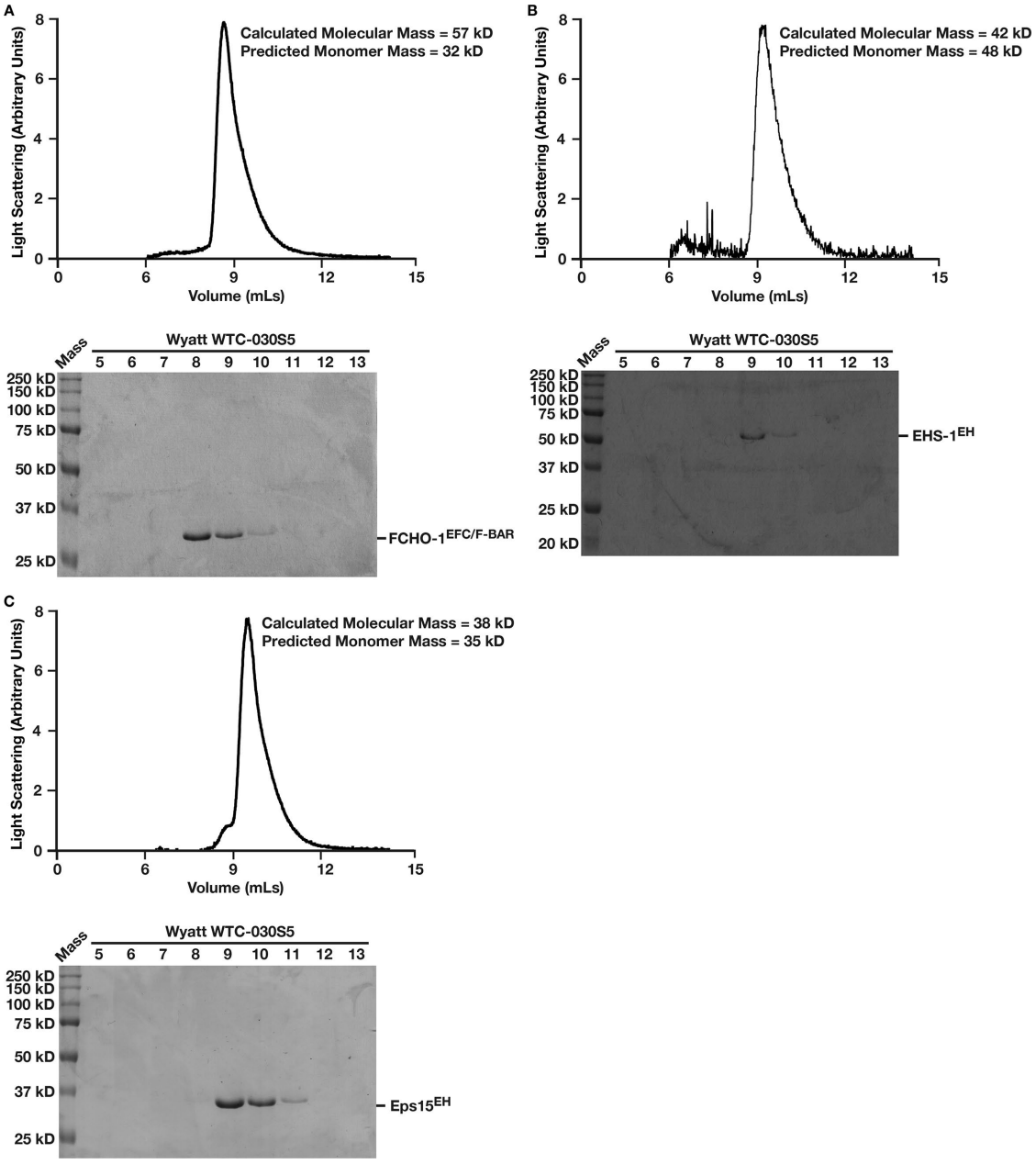

FIGURE 4: The Eps15 EH domain does not require self-association to bind membranes. Purified, recombinant domains of (A) FCHO-1 (EFC/F-BAR), (B) EHS-1 (EH), or (C) mouse Eps15 (EH) were separated over a gel filtration column coupled to a multiangle light scattering device. Light scattering profiles are plotted; eluted fractions were separated by SDS–PAGE and stained using Coomassie to highlight the elution profile of each protein.

did not alter the plasma membrane distribution of the EHS-1 EH domain (Figure 3B). Taken together, these data strongly suggest that the EHS-1 EH domains possess a preference for PI4,5P_2 in membrane binding and are capable of associating with NPF-containing factors and PI4,5P_2 simultaneously. Consistent with this idea, coflotation of the EHS-1 EH domain was not altered by coincubation with the carboxyl-terminal region of *C. elegans* epsin (EPN-1), which harbors numerous NPF motifs (Figure 3G).

Previous data indicate that EFC/F-BAR domains form dimers, which enables them to bind and bend membranes (Henne *et al.*, 2007). We confirmed homodimerization of the FCHO-1 EFC/F-BAR domain using size exclusion chromatography coupled to multiangle light scattering (Figure 4A). Using the same approach, we investigated whether the tandem EH domains in *C. elegans* EHS-1 and mouse Eps15 undergo oligomerization in solution. Unlike the EFC/F-BAR domain, the EH domains failed to self-associate in solution and exhibited molecular masses consistent with monodisperse monomers (Figure 4, B and C).

Eps15-mediated membrane binding and bending is essential in the absence of the Fcho1 EFC/F-BAR domain

If EHS-1 acts redundantly with FCHO-1, its EH domains should exhibit the ability to deform and tubulate membranes, as has been shown for the EFC/F-BAR domain (Henne *et al.*, 2007, 2010). To address this issue, we used a cellular tubulation assay in which we overexpressed GFP fusions to either the FCHO-1 EFC/F-BAR domain

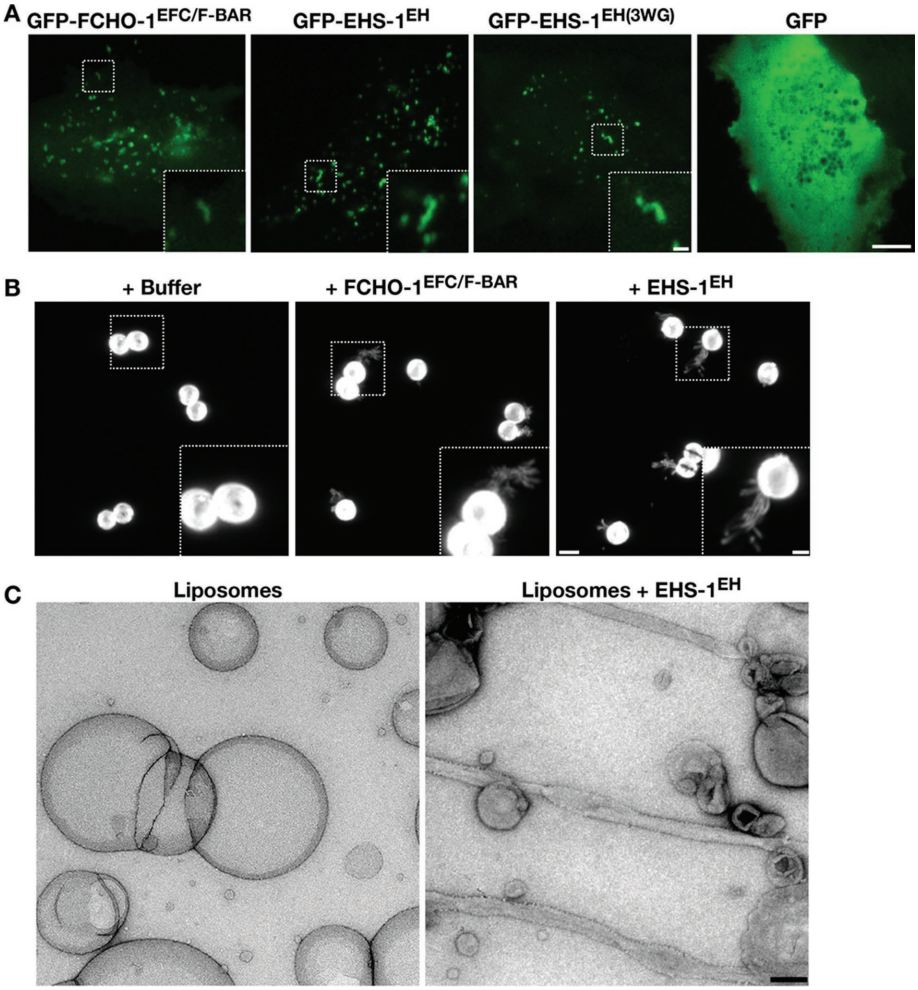

FIGURE 5: The Eps15 EH domain drives membrane bending in cells and in vitro. (A) RPE1 cells transiently overexpressing a variety of GFP fusion proteins were imaged using swept-field confocal optics. Scale bars, 5 μm (main image), 1 μm (zoomed inset). Data shown are representative of >30 cells imaged for each condition in three independent experiments. (B) Supported bilayers with SUPER templates were incubated with buffer alone, the EFC/F-BAR domain of FCHO-1 (2 μM), or the tandem EH domain of EHS-1 (2 μM) and imaged using swept-field confocal optics. A maximum intensity projection of a serial *z*-series (0.2-μm steps) is shown in each case. Data are representative of experiments conducted five times independently. Scale bar, 5 μm. Bottom, right, higher-magnification views of the indicated regions (boxed); scale bar, 1 μm. (C) Liposomes incubated in the presence or absence of the EHS-1 EH domain (1 μM) were imaged using negative-staining electron microscopy. Scale bar, 200 nm. Data shown are representative of multiple fields of view.

or the EHS-1 tandem EH domain in human RPE1 cells. In both cases, we observed the formation of small tubules (~2–3 μm) as well as numerous bright foci at or near the cell periphery (Figure 5A), consistent with previous work using the human Fcho2 EFC/F-BAR domain (Henne *et al.*, 2010). In contrast, overexpression of GFP alone led to only a diffuse signal throughout cells. For a more quantitative measurement of tubulation, we also took advantage of fluid-supported bilayers with excess membrane reservoir (SUPER) templates (Pucadyil and Schmid, 2010). On addition of various proteins to the SUPER templates, we determined the percentage that exhibited membrane tubules. In several independent assays, we found that the EHS-1 EH domains tubulated membranes as efficiently as the FCHO-1 EFC/F-BAR domain (Figure 5B). We further examined EH domain–mediated membrane tubulation using electron microscopy. On addition of the EHS-1 tandem EH domain, large unilamellar vesicles were converted into tubules that exhibited variable widths (Figure 5C). Membrane tubes appeared to be decorated with particles. However, given their lack of symmetry, further structural characterization was not possible.

In contrast to the effects of the purified EH domains, full-length EHS-1, which forms homodimers in solution, exhibited a relatively weak ability to promote membrane tubulation in the SUPER template assay (Figure 6A). Similarly, full-length ITSN-1 was ineffective at promoting membrane tubulation (Figure 6A). However, a complex of EHS-1 and ITSN-1 generated by mixing the proteins and isolating heterodimers by size exclusion chromatography (Figure 6B) deformed membranes similarly to the isolated EH domains (Figure 6, A and C). Together our data indicate that heterodimers of EHS-1 and ITSN-1 exhibit distinct membrane-bending properties compared with EHS-1 homodimers, potentially due to conformational autoinhibition that results from EHS-1 self-association in the absence of other binding partners in vitro. In addition, these findings offer an additional explanation for the poor viability of embryos lacking both FCHO-1 and ITSN-1, as the remaining EHS-1 homodimers in this strain background would not be able to bend membranes as efficiently as heterodimers of EHS-1 and ITSN-1.

Collectively our genetic and biochemical data point to an overlapping function for FCHO-1 and EHS-1 in membrane binding and bending. To test this further, we generated a strain that lacks both FCHO-1 and EHS-1 but ubiquitously expresses a truncated form of FCHO-1 that lacks its amino-terminal EFC/F-BAR domain (FCHO-1$^{288–968}$). In *fcho-1* null animals, FCHO-1$^{288–968}$ fully complements defects in endocytosis, morphogenesis, and embryo viability (Figure 6D; Hollopeter *et al.*, 2014). In contrast, the penetrant embryo lethality observed in *fcho-1/ehs-1* double-mutant animals was not rescued by expression of FCHO-1$^{288–968}$, suggesting that the EFC/F-BAR domain plays an important function when EHS-1 is absent (Figure 6D). These data argue that the FCHO-1 EFC/F-BAR domain and the EHS-1 EH domains play redundant roles in membrane binding and bending during initial phases of clathrin-mediated endocytosis.

Eps15 acts redundantly with Fcho1 to stabilize AP-2 at the plasma membrane

Previous studies highlighted an important role for FCHO-1 in regulating the stability of coated pits (Cocucci *et al.*, 2012; Umasankar *et al.*, 2014). To confirm this effect in *C. elegans* embryos, we used animals stably expressing very low levels of a GFP-tagged form of APA-2 (Figure 7A) and examined its cell surface distribution at a specific time after embryo fertilization, when clathrin-mediated

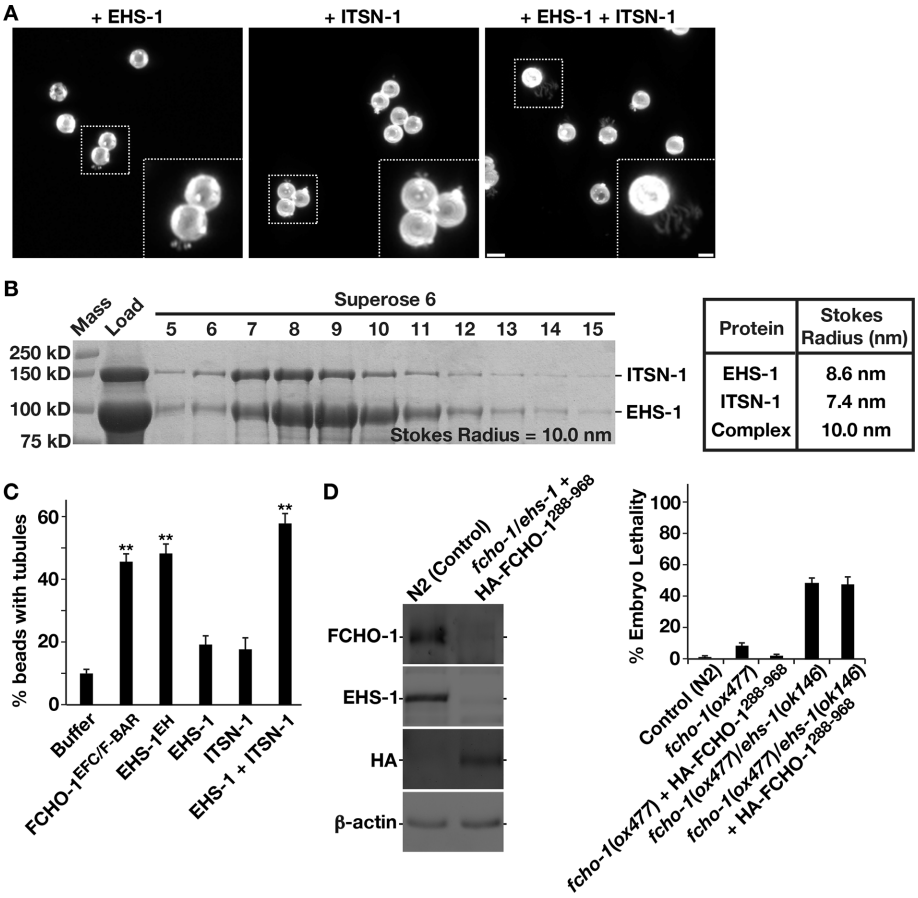

FIGURE 6: Heterodimers of EHS-1 and ITSN-1 promote membrane bending in vitro. (A) SUPER templates were incubated with full-length EHS-1 (2 μM), full-length ITSN-1 (2 μM), or a mixture of the two proteins (1 μM each) and imaged using swept-field confocal optics. A maximum intensity projection of a serial *z*-series (0.2-μm steps) is shown in each case. Data are representative of experiments conducted five times independently. Scale bar, 5 μm. Bottom, right, higher-magnification views of the indicated regions (boxed); scale bar, 1 μm. (B) Independently purified EHS-1 and ITSN-1 were mixed briefly and applied onto a Superose 6 gel filtration column. Based on their elution profiles and those of known standards, an average Stokes radius was calculated for the complex. Right, table showing the Stokes radii of EHS-1 alone, ITSN-1 alone, and the EHS-1/ITSN-1 complex. Data shown are representative of three independent experiments. (C) Quantification of the number of SUPER templates exhibiting tubulation upon addition of various proteins. Error bars represent mean ± SEM. $^{**}p < 0.01$ compared with buffer alone, calculated using a paired *t* test. (D) Gravid adults ($n = 30$) of each genotype indicated were pooled and solubilized in SDS-containing sample buffer. Left, boiled extracts were resolved by SDS–PAGE and immunoblotted using the antibodies indicated. Data shown are representative of three independent experiments. Control and mutant animals were segregated individually onto plates as synchronized adults and allowed to produce progeny for 24 h. Right, percentage of embryos that failed to hatch was determined in each case. Error bars represent mean ± SEM; five replicates each.

endocytosis is elevated (~23 min after ovulation; Wang and Audhya, 2014). Consistent with prior work in mammalian cells, we observed a decline in the number of endocytic pits harboring AP-2 in *fcho-1* null animals, and the majority of AP-2– labeled structures exhibited a reduced size relative to control embryos (Figure 7, B and C; Cocucci *et al.*, 2012). To test whether FCHO-1 and heterodimers of EHS-1 and ITSN-1 function redundantly in regulating the stability of coated pits, we examined AP-2 accumulation at the embryo cortex in *fcho-1/ehs-1/itsn-1* triple-mutant animals. Our results identified a further significant decline in AP-2 assembly at the plasma membrane in this strain background compared with *fcho-1* or *ehs-1* single-mutant animals, highlighting another important overlapping function for FCHO-1 and EHS-1/ITSN-1 in clathrin-mediated endocytosis (Figure 7, C and D). We also considered the possibility that EHS-1 acts redundantly with FCHO-1 to activate the AP-2 complex. However, in contrast to *fcho-1/apa-2* double-mutant animals, which do not exhibit a synthetic genetic interaction with one another (Hollopeter *et al.*, 2014), we found that *ehs-1/apa-2* double-mutant embryos were not viable (Figure 7E). Together these data suggest that FCHO-1 and EHS-1 do not share all of the same functions upstream of AP-2 but instead work in unison to facilitate its stable recruitment, maintenance, and/or function at clathrin-coated pits.

DISCUSSION

The number of accessory factors implicated in clathrin-mediated vesicle transport far exceeds that involved in other coat-driven trafficking pathways (e.g., COPI and COPII), at least in part due to the numerous unique donor membranes (plasma membrane, Golgi, and endosomes) with which clathrin has been shown to associate (Traub, 2005). Nevertheless, internalization events from the cell surface alone can use more than a dozen adaptors, many of which have specific clientele, whereas others appear to be more promiscuous (Traub and Bonifacino, 2013). Unlike other metazoans, *C. elegans* can tolerate the loss of any individual endocytic clathrin adaptor protein during embryo development, enabling detailed genetic analysis of their overlapping contributions in vivo. This attribute has enabled us to define for the first time a conserved membrane-binding/bending activity associated with Eps15 that had been previously overlooked.

Over the past decade, a substantial effort has been made to determine the sequence of events that enable a clathrin-coated vesicle to form at the plasma membrane. The spatiotemporal accumulation and action of >60 proteins at sites of clathrin-mediated endocytosis have been analyzed, highlighting roles in initiation, maturation, cargo recruitment, membrane bending, vesicle scission, and vesicle uncoating (Merrifield and Kaksonen, 2014). The large number of membrane-remodeling factors involved suggests that clathrin assembly alone is inadequate to efficiently drive vesicle formation in vivo. This idea contrasts with in vitro evidence, which demonstrated previously that clathrin assembly in the absence of membrane-tubulating proteins is sufficient to generate spherical buds on large liposomes (Dannhauser and Ungewickell, 2012). In this case, clathrin was directed onto membranes via the intrinsically disordered region of epsin, which was artificially tethered to liposomes without its membrane-binding ENTH domain. However, recent data indicate that intrinsically disordered domains, including the region of epsin used to reconstitute clathrin-coated

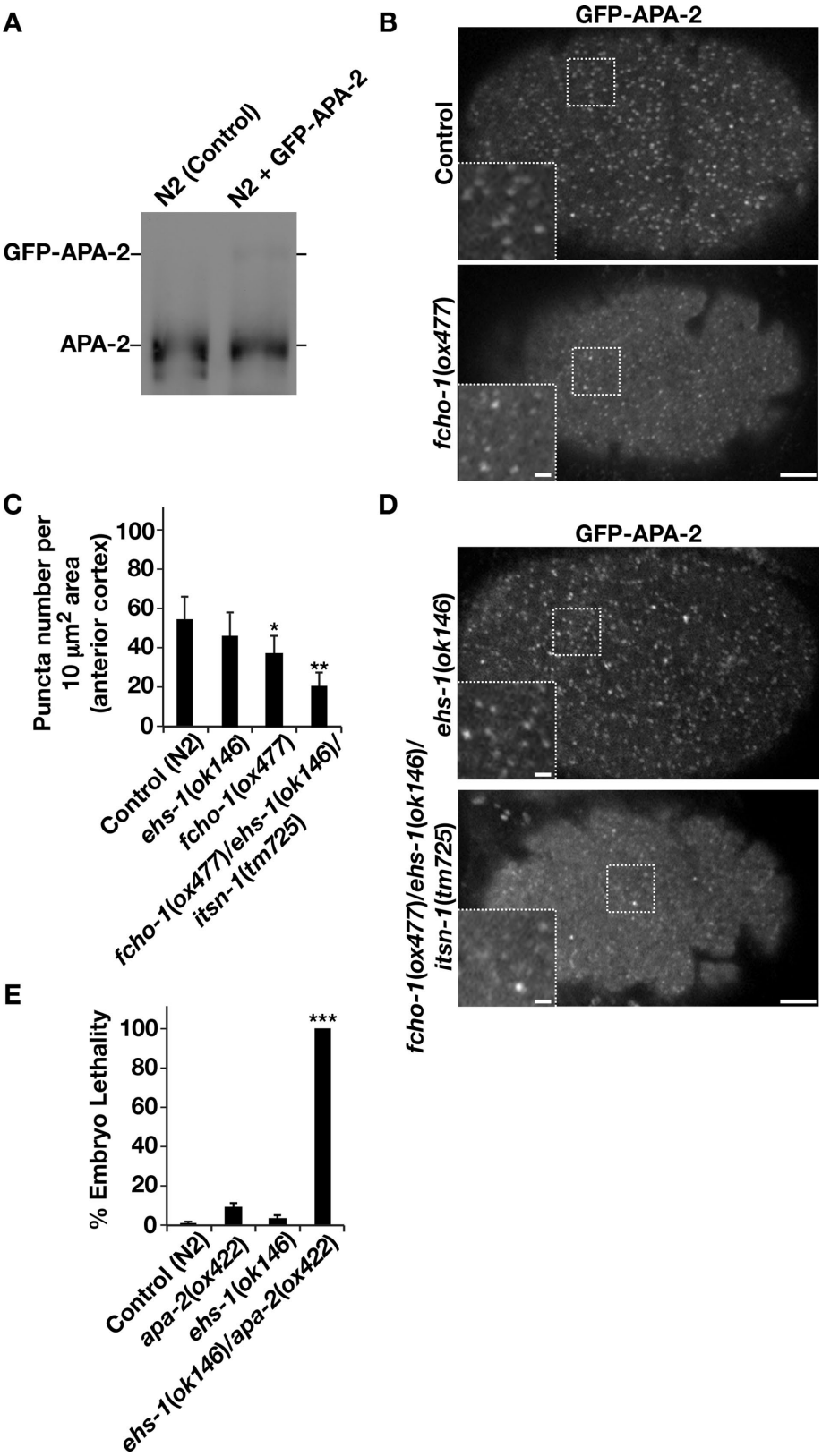

FIGURE 7: Eps15 and Fcho1 function redundantly to facilitate clathrin-mediated endocytosis. (A) Gravid adults (n = 30) of each genotype indicated were pooled and solubilized in SDS-containing sample buffer. Boiled extracts were resolved by SDS–PAGE and immunoblotted using APA-2 antibodies. Data shown are representative of three independent experiments. (B) Embryos stably expressing low levels of GFP-tagged APA-2 were imaged in utero using swept-field confocal optics at the cell cortex. Scale bar, 5 μm. Bottom, right, higher-magnification views of the indicated regions (boxed); scale bar, 1 μm. Data shown are representative of >30 embryos imaged in three independent experiments for each condition. (C) Quantification of the number of puncta per unit area at the anterior embryo cortex in various genetic backgrounds. Error bars represent mean ± SEM. $^{**}p < 0.01$ compared with control and $^{*}p < 0.05$ compared with control, calculated using a paired t test. At least 50 different areas in 30 individual embryos were examined for each condition. (D) Early-stage embryos stably expressing low levels of GFP-tagged APA-2 in the *ehs-1* single-mutant or *fcho-1/ehs-1/itsn-1* triple-mutant background were imaged in utero using swept-field confocal optics at the cell cortex. Scale bar, 5 μm. Bottom, left, higher-magnification views of the indicated regions (boxed); scale bar, 1 μm. Data shown are representative of >30 embryos imaged in three independent experiments for each condition (E) Control and mutant animals were segregated individually onto plates as synchronized adults and allowed to produce progeny for 24 h. The percentage of embryos that failed to hatch was determined in each case. For analysis of the *ehs-1/apa-2* double-mutant condition, animals lacking APA-2 but harboring one intact *EHS-1* allele were analyzed. These animals yielded progeny that exhibited ~50% lethality. All viable progeny continued to express *EHS-1* in a heterozygous manner, indicating that the *ehs-1/apa-2* mutant combination is 100% lethal. Error bars represent mean ± SEM; five replicates each. $^{***}p < 0.001$ compared with *apa-2*(*ox422*) or *ehs-1*(*ok146*) animals, calculated using a paired t test.

bud formation in vitro, are potent drivers of membrane curvature via molecular crowding and the generation of steric pressure (Stachowiak *et al.*, 2012; Busch *et al.*, 2015). Thus it remains to be seen whether clathrin assembly, in the absence of other proteins that bind and remodel membranes, can directly lead to vesicle budding. Instead, it may be more likely that membrane-bending factors work in concert with clathrin to drive this process, both early, during membrane invagination, and later, during subsequent steps of vesicle formation and ultimately scission.

Based on overexpression studies, all three components of the FEI complex have been suggested to act during the initial stages of clathrin-mediated endocytosis in animal cells, immediately after initiation of coat assembly (Henne *et al.*, 2010). These data are consistent with live-cell imaging experiments in yeast examining the endogenous fungal homologues of Fcho1 (Syp1p) and Eps15 (Ede1p), which arrive before other membrane-bending factors, including epsin (Ent1/2p) and AP180/CALM (Yap1801/2p;

Stimpson *et al.*, 2009). Despite the close biochemical relationship between the FEI subunits (Mayers *et al.*, 2013), which would predict interdependence for their functions and/or localizations, we found that Fcho1 and Eps15 exhibit significant redundancy and can act independently of one another. In an analogous manner, we and others have shown that individual components of the AP-2 complex, a stable heterotetramer, can be eliminated in *C. elegans* with only modest consequences, whereas combined loss of both AP-2 hemicomplexes is lethal (Gu *et al.*, 2013). These data suggest the possibility that the FEI complex, like the AP-2 complex, functions most efficiently when all components are present, but the removal of a single player can be tolerated due to the plasticity of the system as a whole.

Our findings also raise the question of what unique role the FEI complex may play during the first steps of coated pit formation. One possibility is that Fcho1, Eps15, and intersectin collectively facilitate the earliest stages of membrane deformation and help to stabilize a dynamic clathrin lattice, which must undergo continuous bending and remodeling as its composition shifts from primarily hexagons to acquiring pentagons (Avinoam *et al.*, 2015). Our findings suggest that in the absence of one membrane-bending protein, such as Fcho1, the others (Eps15 and intersectin) remain largely capable of carrying out this activity. However, when all three accessory factors are removed, clathrin-mediated endocytosis is severely attenuated, potentially due to the inability of the remaining endocytic adaptors to create a membrane topology compatible with the initial steps of clathrin lattice bending.

Alternatively, the membrane-binding capability of Eps15 may be important to direct its distribution at clathrin-coated pits. Unlike several other accessory factors at sites of clathrin-mediated endocytosis, both Eps15 and Fcho1 accumulate at the rim of growing invaginations, potentially acting to stabilize the highly bent membrane as it progresses toward a fission intermediate (Tebar *et al.*, 1996; Henne *et al.*, 2010). Epsin, another accessory factor capable of membrane tubulation, similarly associates with the rim (Saffarian *et al.*, 2009). These data raise the possibility that Eps15, Fcho1, and epsin (as well as other membrane-binding accessory proteins) act as curvature sensors and scaffold-interacting partners at the rim of coated pits to facilitate vesicle maturation, cargo incorporation, and/or other activities necessary during endocytosis. Irrespective of the precise function of Eps15 membrane binding (e.g., sensing vs. bending), our findings argue that it plays an essential, redundant role with the Fcho1 EFC/F-BAR domain to promote clathrin-mediated vesicle formation at the plasma membrane.

MATERIALS AND METHODS

Antibodies, immunofluorescence, and live-cell/animal imaging

C. elegans APA-2 polyclonal antibodies were outsourced for production in rabbits (Pacific Immunology, Ramona, CA). Each rabbit was immunized with a fragment of APA-2 (amino acids 619–925) fused to glutathione *S*-transferase (GST), which was produced in *Escherichia coli*. Antibodies were affinity purified from serum by binding to columns of the same antigen after removal of the GST tag. Antibodies directed against FCHO-1, EHS-1, and ITSN-1 have been described (Mayers *et al.*, 2013), and antibodies against β-actin (Sigma-Aldrich, St. Louis, MO) and the human influenza hemagglutinin (HA) tag (BioLegend, San Diego, CA) were obtained from commercial sources.

Confocal images were acquired on a swept-field confocal microscope (Nikon Ti-E) equipped with a Nikon 60×, 1.4 numerical aperture Planapo oil objective lens and a CoolSNAP HQ2 charge-coupled device camera. Immunofluorescence of fixed embryos was performed using directly labeled rabbit antibodies at a final concentration of 1 µg/ml (Mayers *et al.*, 2013). At least 40 sections (0.2-µm steps) were acquired, and individual planes from each imaging series are shown unless otherwise indicated. Human RPE1 cells were plated on 35-mm glass-bottom dishes and imaged live. Briefly, 40–60 *Z*-sections (0.2-µm steps) were acquired. Acquisition parameters and image analysis were performed using Nikon Elements software. For experiments involving SigD expression, a final concentration of 10 ng/ml doxycycline was used, and cells were imaged 24 h after induction. For live imaging of GFP-APA-2, *C. elegans* were immobilized and 10 cortical *Z*-sections (0.2-µm steps) were acquired 23 min after oocyte ovulation in utero (Wang *et al.*, 2014). Individual planes ~1 µm from the eggshell were chosen for quantification of APA-2 puncta at the cortex. Only puncta that reached a minimal threshold of fluorescence intensity (after background subtraction) were used for quantification. To calculate the relative fluorescence intensities of endogenous EHS-1 in four-cell-stage embryos, an average intensity along the border between the ABa and ABp cells was first calculated (after background subtraction). All images shown are representative of experiments conducted more than three times independently.

C. elegans strain growth, maintenance, and RNAi

All *C. elegans* strains used in this study were derived from the Bristol strains N2 and described previously (Pant *et al.*, 2009; Kang *et al.*, 2013; Mayers *et al.*, 2013; Hollopeter *et al.*, 2014), and deletion mutants were obtained from the *Caenorhabditis* Genetics Center or the Mitani lab through the National Bio-Resource Project (Japan). Double-stranded RNA (dsRNA) was synthesized from templates prepared using specific primers to amplify N2 genomic DNA (Witte *et al.*, 2011). Primer design was based on previous high-throughput studies (Sönnichsen *et al.*, 2005). For RNAi experiments, early L4-stage hermaphrodites were soaked in dsRNA for 24 h at 20°C within a humidified chamber. Animals were then allowed to recover on nematode growth medium plates for 48 h before embryo lethality analysis, as described previously (Mayers *et al.*, 2013).

Mammalian cell culture, transfections, and transcription activator–like effector nuclease–mediated genome editing

RPE1 cells were grown in DME/F-12 supplemented with 10% fetal bovine serum, penicillin/streptomycin, and L-glutamine (Invitrogen, Carlsbad, CA) and maintained at 37°C and 5% CO_2. Plasmid transfections were conducted using FuGENE HD (Promega, Madison, WI) as recommended by the manufacturer.

To generate clonal doxycycline-inducible cell lines to express untagged forms of the bacterial phosphatase SigD, we used a transcription activator–like effector nuclease (TALEN)–mediated targeting system that incorporates transgenes at the *AAVS1* locus (Qian *et al.*, 2014). In each case, the cassette (SigD followed by an internal ribosome entry site and red fluorescent protein [RFP]) was electroporated into human RPE1 cells together with the two *AAVS1*-specific TALEN plasmids at a ratio of 8:1:1, and the cells were treated with puromycin (1 µg/ml) for ~3 wk. After puromycin selection, cells were sorted based on RFP expression after a 12-h induction with 10 ng/ml doxycycline. Cells stably expressing low levels of wild-type (WT) and mutant forms of EHS-1^{EH}-GFP and GFP-C2 (C2 domain from bovine lactadherin) were generated in the sorted SigD^{WT} or SigD^{C460S} cell lines by retroviral infection followed by selection with blasticidin.

Protein expression, purification, mass determinations, and immunoblotting

Recombinant protein expression was performed using BL21 *E. coli*, and purification was conducted by using glutathione agarose beads

for GST fusions proteins or nickel affinity resin for hexahistidine (His_6)-SUMO-tagged proteins. All proteins used in this study were eluted and purified into a common buffer (50 mM 4-(2-hydroxyethyl)-1-piperazineethanesulfonic acid [HEPES], pH 7.6, 100 mM NaCl, 1 mM $MgCl_2$, and 10% glycerol). Precision or Sumo protease was used to remove the GST or His_6-Sumo tag, respectively. Cleaved proteins were applied onto a MonoQ ion exchange column (GE, Boston, MA) and a Superdex S200 column (GE) for further purification. Purified proteins were subjected to size-exclusion chromatography coupled to a Wyatt mini-DAWN TREOS three-angle light scattering detector. Data were collected at flow rate of 0.5 ml/min and analyzed using ASTRA software to determine molecular mass (Schuh *et al.*, 2015). Immunoblotting of *C. elegans* extracts was performed as described (Witte *et al.*, 2011). For calculation of Stokes radii, recombinant proteins and standards were applied onto a Superose 6 gel filtration column and calculations made as described (Mayers *et al.*, 2013).

The following protein domains were generated recombinantly for binding studies: ITSN-1 tandem EH domain (amino acids [aa] 1–265), ITSN-1 SH3 domain (aa 662–1086), FCHO-1 EFC/F-BAR domain (aa 1–276), EHS-1 tandem EH domain (aa 1–448), EHS-1 EH1 domain (aa 1–130), EHS-1 EH1-EH2 domain (aa 1–290), EHS-1 EH3 domain (aa 291–448), EHS-1 EH2-EH3 domain (aa 131–448), mouse Eps15 tandem EH domain (aa 1–325), and EPN-1 NPF domain (aa 314–469).

Synthetic liposome generation, liposome coflotation, SUPER template assays, and electron microscopy

Liposomes were generated as described previously (Schuh *et al.*, 2015). Briefly, five phospholipids obtained from Avanti Polar Lipids (Alabaster, AL; 1-palmitoyl-2-oleoyl-*sn*-glycero-3-phosphocholine [POPC], 1-palmitoyl-2-oleoyl-*sn*-glycero-3-phosphoethanolamine [POPE], 1-palmitoyl-2-oleoyl-*sn*-glycero-3-phospho-L-serine [POPS], 1,2-dipalmitoyl-*sn*-glycero-3-phosphoethanolamine-*N*-(lissamine rhodamine B sulfonyl) [Rhod-PE], and $PI4,5P_2$) were mixed at different molar ratios to generate liposomes with varying concentrations of negatively charged lipids. The lipids were dried and resuspended in 50 mM HEPES (pH 7.6), 100 mM NaCl, and 1 mM $MgCl_2$ and extruded through a nitrocellulose filter with 0.1-μm pores.

Liposome coflotation assays were conducted as described (Schuh *et al.*, 2015). Briefly, proteins were incubated with liposomes (3 mM) on ice for 30 min before being mixed with 125 μl of 80% Accudenz (wt/vol in 50 mM HEPES, pH 7.6, 100 mM NaCl, and 1 mM $MgCl_2$). The mixture was transferred into centrifuge tubes (Beckman, Brea, CA) and sequentially overlaid with 200 μl each of 35 and 30% Accudenz, followed by 20 μl of buffer (50 mM HEPES, pH 7.6, 100 mM NaCl, and 1 mM $MgCl_2$). Samples were centrifuged in a SW-55 rotor (Beckman) for 2.5 h at 48,000 rpm. The vesicles were collected from the 0/30% Accudenz interface in 40 μl, and recovery was quantified based on rhodamine fluorescence. Normalized samples were separated by SDS–PAGE and subsequently silver stained.

SUPER templates were generated as described previously (Pucadyil and Schmid, 2010). Briefly, liposomes (POPC, 52%; POPE, 29%; POPS, 15%; $PI4,5P_2$, 3%; Rhod-PE, 1%) were incubated with 5-μm silica beads (Bangs Laboratories, Fishers, IN) for 30 min in high-salt buffer (50 mM HEPES, pH 7.6, 1 M NaCl, and 1 mM dithiothreitol [DTT]). The reaction was centrifuged for 30 s at 600 × *g* to pellet the SUPER templates, and the high-salt buffer was removed. The templates were washed three times with water and subsequently resuspended in low-salt buffer (50 mM HEPES, pH 7.6, 100 mM NaCl, and 1 mM DTT) twice. Templates were brought up in 100 μl to generate a 10× stock. Proteins (2 μM) were incubated with templates (1× final concentration) for 15 min at room temperature before the reaction was imaged using a gelatin-coated chamber. For assays using both EHS-1 and ITSN-1, each protein was present at a concentration of 1 μM. To quantify the degree of in vitro tubulation achieved for each condition, only tubules exhibiting a length of >5 μm were counted. Electron microscopy studies to examine liposome tubulation were conducted as described (Guerrier *et al.*, 2009), using 1 μM EHS-1^{EH}.

ACKNOWLEDGMENTS

We thank Adam Frost (University of California, San Francisco, San Francisco, CA) for consulting on electron microscopy studies and members of the Audhya lab for making suggestions and critically reading the manuscript. This work was supported in part by Grant GM088151 from the National Institutes of Health to A.A.

REFERENCES

Avinoam O, Schorb M, Beese CJ, Briggs JA, Kaksonen M (2015). ENDOCYTOSIS. Endocytic sites mature by continuous bending and remodeling of the clathrin coat. Science 348, 1369–1372.

Benmerah A, Bégue B, Dautry-Varsat A, Cerf-Bensussan N (1996). The ear of alpha-adaptin interacts with the COOH-terminal domain of the Eps 15 protein. J Biol Chem 271, 12111–12116.

Busch DJ, Houser JR, Hayden CC, Sherman MB, Lafer EM, Stachowiak JC (2015). Intrinsically disordered proteins drive membrane curvature. Nat Commun 6, 7875.

Carbone R, Fré S, Iannolo G, Belleudi F, Mancini P, Pelicci PG, Torrisi MR, Di Fiore PP (1997). eps15 and eps15R are essential components of the endocytic pathway. Cancer Res 57, 5498–5504.

Chen H, Fre S, Slepnev VI, Capua MR, Takei K, Butler MH, Di Fiore PP, De Camilli P (1998). Epsin is an EH-domain-binding protein implicated in clathrin-mediated endocytosis. Nature 394, 793–797.

Cocucci E, Aguet F, Boulant S, Kirchhausen T (2012). The first five seconds in the life of a clathrin-coated pit. Cell 150, 495–507.

Conner SD, Schmid SL (2003). Differential requirements for AP-2 in clathrin-mediated endocytosis. J Cell Biol 162, 773–779.

Dannhauser PN, Ungewickell EJ (2012). Reconstitution of clathrin-coated bud and vesicle formation with minimal components. Nat Cell Biol 14, 634–639.

de Beer T, Hoofnagle AN, Enmon JL, Bowers RC, Yamabhai M, Kay BK, Overduin M (2000). Molecular mechanism of NPF recognition by EH domains. Nat Struct Biol 7, 1018–1022.

Dove SK, Dong K, Kobayashi T, Williams FK, Michell RH (2009). Phosphatidylinositol 3,5-bisphosphate and Fab1p/PIKfyve in endo-lysosome function. Biochem J 419, 1–13.

Fazioli F, Minichiello L, Matoskova B, Wong WT, Di Fiore PP (1993). eps15, a novel tyrosine kinase substrate, exhibits transforming activity. Mol Cell Biol 13, 5814–5828.

Gu M, Liu Q, Watanabe S, Sun L, Hollopeter G, Grant BD, Jorgensen EM (2013). AP2 hemicomplexes contribute independently to synaptic vesicle endocytosis. Elife 2, e00190.

Gu M, Schuske K, Watanabe S, Liu Q, Baum P, Garriga G, Jorgensen EM (2008). Mu2 adaptin facilitates but is not essential for synaptic vesicle recycling in Caenorhabditis elegans. J Cell Biol 183, 881–892.

Guerrier S, Budd JC, Sassa T, Gresset A, Jordan NV, Cheng K, Jin WL, Frost A, Polleux F (2009). The F-BAR domain of srGAP2 induces membrane protrusions required for neuronal migration and morphogenesis. Cell 138, 990–1004.

Haffner C, Takei K, Chen H, Ringstad N, Hudson A, Butler MH, Salcini AE, Di Fiore PP, De Camilli P (1997). Synaptojanin 1: localization on coated endocytic intermediates in nerve terminals and interaction of its 170 kDa isoform with Eps15. FEBS Lett 419, 175–180.

Henne WM, Boucrot E, Meinecke M, Evergren E, Vallis Y, Mittal R, McMahon HT (2010). FCHo proteins are nucleators of clathrin-mediated endocytosis. Science 328, 1281–1284.

Henne WM, Kent HM, Ford MG, Hegde BG, Daumke O, Butler PJ, Mittal R, Langen R, Evans PR, McMahon HT (2007). Structure and analysis of

FCHo2 F-BAR domain: a dimerizing and membrane recruitment module that effects membrane curvature. Structure 15, 839–852.
Hollopeter G, Lange JJ, Zhang Y, Vu TN, Gu M, Ailion M, Lambie EJ, Slaughter BD, Unruh JR, Florens L, *et al*. (2014). The membrane-associated proteins FCHo and SGIP are allosteric activators of the AP2 clathrin adaptor complex. Elife 3, e03648.
Jackson LP, Kelly BT, McCoy AJ, Gaffry T, James LC, Collins BM, Höning S, Evans PR, Owen DJ (2010). A large-scale conformational change couples membrane recruitment to cargo binding in the AP2 clathrin adaptor complex. Cell 141, 1220–1229.
Kaksonen M, Toret CP, Drubin DG (2005). A modular design for the clathrin- and actin-mediated endocytosis machinery. Cell 123, 305–320.
Kang YL, Yochem J, Bell L, Sorensen EB, Chen L, Connera SD (2013). Caenorhabditis elegans reveals a FxNPxY-independent low-density lipoprotein receptor internalization mechanism mediated by epsin1. Mol Biol Cell 24, 308–318.
Katoh M, Katoh M (2004). Identification and characterization of human FCHO2 and mouse Fcho2 genes in silico. Int J Mol Med 14, 327–331.
Kirchhausen T, Owen D, Harrison SC (2014). Molecular structure, function, and dynamics of clathrin-mediated membrane traffic. Cold Spring Harb Perspect Biol 6, a016725.
Koh TW, Korolchuk VI, Wairkar YP, Jiao W, Evergren E, Pan H, Zhou Y, Venken KJ, Shupliakov O, Robinson IM, *et al*. (2007). Eps15 and Dap160 control synaptic vesicle membrane retrieval and synapse development. J Cell Biol 178, 309–322.
Martina JA, Bonangelino CJ, Aguilar RC, Bonifacino JS (2001). Stonin 2: an adaptor-like protein that interacts with components of the endocytic machinery. J Cell Biol 153, 1111–1120.
Mayers JR, Wang L, Pramanik J, Johnson A, Sarkeshik A, Wang Y, Saengsawang W, Yates JR 3rd, Audhya A (2013). Regulation of ubiquitin-dependent cargo sorting by multiple endocytic adaptors at the plasma membrane. Proc Natl Acad Sci USA 110, 11857–11862.
Merrifield CJ, Kaksonen M (2014). Endocytic accessory factors and regulation of clathrin-mediated endocytosis. Cold Spring Harb Perspect Biol 6, a016733.
Naslavsky N, Rahajeng J, Chenavas S, Sorgen PL, Caplan S (2007). EHD1 and Eps15 interact with phosphatidylinositols via their Eps15 homology domains. J Biol Chem 282, 16612–16622.
Pant S, Sharma M, Patel K, Caplan S, Carr CM, Grant BD (2009). AMPH-1/Amphiphysin/Bin1 functions with RME-1/Ehd1 in endocytic recycling. Nat Cell Biol 11, 1399–1410.
Pozzi B, Amodio S, Lucano C, Sciullo A, Ronzoni S, Castelletti D, Adler T, Treise I, Betsholtz IH, Rathkolb B, *et al*. (2012). The endocytic adaptor Eps15 controls marginal zone B cell numbers. PLoS One 7, e50818.
Pucadyil TJ, Schmid SL (2010). Supported bilayers with excess membrane reservoir: a template for reconstituting membrane budding and fission. Biophys J 99, 517–25.
Qian K, Huang CT, Chen H, Blackbourn LW 4th, Chen Y, Cao J, Yao L, Sauvey C, Du Z, Zhang SC (2014). A simple and efficient system for regulating gene expression in human pluripotent stem cells and derivatives. Stem Cells 32, 1230–1238.
Reider A, Barker SL, Mishra SK, Im YJ, Maldonado-Báez L, Hurley JH, Traub LM, Wendland B (2009). Syp1 is a conserved endocytic adaptor that contains domains involved in cargo selection and membrane tubulation. EMBO J 28, 3103–3116.
Saffarian S, Cocucci E, Kirchhausen T (2009). Distinct dynamics of endocytic clathrin-coated pits and coated plaques. PLoS Biol 7, e1000191.
Salcini AE, Hilliard MA, Croce A, Arbucci S, Luzzi P, Tacchetti C, Daniell L, De Camilli P, Pelicci PG, Di Fiore PP, *et al*. (2001). The Eps15 C. elegans homologue EHS-1 is implicated in synaptic vesicle recycling. Nat Cell Biol 3, 755–760.
Schuh AL, Hanna M, Quinney K, Wang L, Sarkeshik A, Yates JR 3rd, Audhya A (2015). The VPS-20 subunit of the endosomal sorting complex ESCRT-III exhibits an open conformation in the absence of upstream activation. Biochem J 466, 625–637.
Sengar AS, Wang W, Bishay J, Cohen S, Egan SE (1999). The EH and SH3 domain Ese proteins regulate endocytosis by linking to dynamin and Eps15. EMBO J 18, 1159–1171.
Shimada A, Yamaguchi A, Kohda D (2016). Structural basis for the recognition of two consecutive mutually interacting DPF motifs by the SGIP1 μ homology domain. Sci Rep 6, 19565.
Sönnichsen B, Koski LB, Walsh A, Marschall P, Neumann B, Brehm M, Alleaume AM, Artelt J, Bettencourt P, Cassin E, *et al*. (2005). Full-genome RNAi profiling of early embryogenesis in Caenorhabditis elegans. Nature 434, 462–469.
Stachowiak JC, Schmid EM, Ryan CJ, Ann HS, Sasaki DY, Sherman MB, Geissler PL, Fletcher DA, Hayden CC (2012). Membrane bending by protein-protein crowding. Nat Cell Biol 14, 944–949.
Stimpson HE, Toret CP, Cheng AT, Pauly BS, Drubin DG (2009). Early-arriving Syp1p and Ede1p function in endocytic site placement and formation in budding yeast. Mol Biol Cell 20, 4640–4651.
Taylor MJ, Perrais D, Merrifield CJ (2011). A high precision survey of the molecular dynamics of mammalian clathrin-mediated endocytosis. PLoS Biol 9, e1000604.
Tebar F, Sorkina T, Sorkin A, Ericsson M, Kirchhausen T (1996). Eps15 is a component of clathrin-coated pits and vesicles and is located at the rim of coated pits. J Biol Chem 271, 28727–28730.
Terebiznik MR, Vieira OV, Marcus SL, Slade A, Yip CM, Trimble WS, Meyer T, Finlay BB, Grinstein S (2002). Elimination of host cell PtdIns(4,5)P(2) by bacterial SigD promotes membrane fission during invasion by Salmonella. Nat Cell Biol 4, 766–773.
Traub LM (2005). Common principles in clathrin-mediated sorting at the Golgi and the plasma membrane. Biochim Biophys Acta 1744, 415–437.
Traub LM (2009). Tickets to ride: selecting cargo for clathrin-regulated internalization. Nat Rev Mol Cell Biol 10, 583–596.
Traub LM, Bonifacino JS (2013). Cargo recognition in clathrin-mediated endocytosis. Cold Spring Harb Perspect Biol 5, a016790.
Trevaskis J, Walder K, Foletta V, Kerr-Bayles L, McMillan J, Cooper A, Lee S, Bolton K, Prior M, Fahey R, *et al*. (2005). Src homology 3-domain growth factor receptor-bound 2-like (endophilin) interacting protein 1, a novel neuronal protein that regulates energy balance. Endocrinology 146, 3757–3764.
Umasankar PK, Ma L, Thieman JR, Jha A, Doray B, Watkins SC, Traub LM (2014). A clathrin coat assembly role for the muniscin protein central linker revealed by TALEN-mediated gene editing. Elife 3, e04137.
Umasankar PK, Sanker S, Thieman JR, Chakraborty S, Wendland B, Tsang M, Traub LM (2012). Distinct and separable activities of the endocytic clathrin-coat components Fcho1/2 and AP-2 in developmental patterning. Nat Cell Biol 14, 488–501.
Wang L, Audhya A (2014). In vivo imaging of C. elegans endocytosis. Methods 68, 518–528.
Wang W, Bouhours M, Gracheva EO, Liao EH, Xu K, Sengar AS, Xin X, Roder J, Boone C, Richmond JE, *et al*. (2008). ITSN-1 controls vesicle recycling at the neuromuscular junction and functions in parallel with DAB-1. Traffic 9, 742–754.
Witte K, Schuh AL, Hegermann J, Sarkeshik A, Mayers JR, Schwarze K, Yates JR 3rd, Eimer S, Audhya A (2011). TFG-1 function in protein secretion and oncogenesis. Nat Cell Biol 13, 550–558.